Biophysical Journal, Volume *117*

Supplemental Information

Plastic Deformation and Fragmentation of Strained Actin Filaments

Anthony C. Schramm, Glen M. Hocky, Gregory A. Voth, Jean-Louis Martiel, and Enrique M. De La Cruz

SUPPORTING MATERIAL

Plastic deformation and fragmentation of strained actin filaments

Authors: Anthony C. Schramm[1], Glen M. Hocky[2], Gregory A. Voth[3], Jean-Louis Martiel[4]*, Enrique M. De La Cruz[1]*

Affiliations:

[1]Department of Molecular Biophysics and Biochemistry, Yale University, New Haven, CT, USA.

[2]Department of Chemistry, New York University, New York, NY

[3]Department of Chemistry, Institute for Biophysical Dynamics, and James Franck Institute, University of Chicago, Chicago, IL

[4]TIMC-IMAG Lab, UMR 5525, Inserm/CNRS/Université Grenoble-Alpes, 38706 La Tronche, France

SUPPLEMENTAL DISCUSSION

Effect of filament length

We chose to simulate 100 nm filaments to compromise between longer filaments and quick simulation time. To test whether this choice had an effect on our conclusions we ran simulations of compressed filaments of 50 (75 nm for bare actin), 100, and 150 nm (Figures S1-S3, Table S4). We used 75 nm instead of 50 nm filaments for actin because the rigidity of the 50 nm filaments led to artifacts (overlapping subunits) when we compressed them. The strain energy of the fragmented interfaces prior to fragmentation are very similar (Table S4). The fragmentation angle and rupture force scale with the filament length, but the trends between the types of filaments remain the same.

Effect of bond density

A very low number of bonds between proteins can lead to spurious behavior in our simulations (e.g. actin subunit overlap) because individual links are free to rotate. A single bond in an interface would be free to sample a number of configurations without any energetic cost, as an extreme example of this. To minimize the frequency of such behavior, we chose a relatively high density of bonds between proteins (Figure S4, Table S5). We ran a series of controls to determine whether this choice had an effect on our experimental results. Low bond density seems to allow filaments to break slightly sooner in the compressive process, with a lower fragmentation angle and pre-fragmentation strain energy. The variance for these measures shown in Table S5 also tend to be higher for the lower bond densities, which is likely due to these interfaces being less uniform. However, the differences in the fragmentation angle and strain energies are much less than between bare actin, cofilactin, and boundaries, so we do not expect this choice of bond density to affect our conclusions.

Effects of boundary placement

We compared simulations where we placed actin-cofilactin boundaries in the center and offset as in the main text (Figure S7). Filaments with a center boundary fragment slightly less effectively (54 ± 21 degrees, for 10 simulations) compared to the offset boundary (49 ± 3 degrees, for 25 simulations). One reason is because of differences in the filament shape (whether the boundary coincides with an area of high curvature). A second reason is that bare actin is stiffer, so a filament with a higher amount of bare actin (75% of the length, in the offset case) will store more energy for a given deformation. This will lead to the boundary breaking sooner.

Effect of cofilin gap size

In our discussion of the bimodal distribution of cofilactin fragmentation angles we have implicated small gaps in a fully-decorated filament as the cause of the more easily fragmented population. In Figure 6 we simulated cofilactin filaments with a single missing cofilin, but it is possible that larger gaps could exist on the filament. We also ran multiple simulations (25 each) to find the rupture angle of filaments with two or three adjacent missing cofilins to compare to the single gap case. We measured filament rupture for cofilactin with gaps of two or three adjacent missing cofilin molecules and found critical angles of 45 ± 14 degrees and 42 ± 13 degrees, respectively. Both of these are close to the fragmentation angle of boundaries that we measured. This is unsurprising, as the stiffness and fragmentation rates of these segments are the same as our measured boundaries. A single missing cofilin seems to more closely resemble the experimental result (a difference of ~20 degrees between the two fragmentation populations (1)), but a more confident assessment would require better structural information for these small gaps to inform our model.

SUPPLEMENTAL METHODS

Filament construction

Elastic bonds comprising protein-protein interfaces are placed between each pair of contacting proteins. Bonds are placed randomly, with a uniform density, over an area defined by the buried solvent accessible surface area (calculated using the calc-surface program accessed using the National Institutes of Health scientific supercomputing resource at http://helixweb.nih.gov/structbio/basic.html, for all atoms but water using a 1.4 Angstrom probe size). The resting length of each bond is set by the initial position, and will differ between bonds due to the ellipsoidal shape of the proteins. The response of the bond to deformation is only dependent on changes in bond length, and not their initial resting length.

The stiffness values are obtained from MD model parameters (Table S1), as follows. Periodic structures of actin filaments were constructed and simulated (2) using the molecular dynamics code NAMD (3). Actin subunits had bound ADP for both bare and cofilactin (cofilin-decorated actin) structures. The systems were allowed to relax for 75 ns (actin) or 175 ns (cofilactin) until the RMSD (root mean squared deviation of backbone atom positions) stabilized. Elastic network models were generated from the next 50 ns (collected every 50 ps), as described previously (2), but coarse-graining the filament to one “bead” per subunit instead of 4. The center of mass of each protein (actin or cofilactin) was connected to all adjacent proteins (up to four actin subunits and two cofilin subunits). The bond stiffness of each was

iteratively adjusted until the fluctuations in the harmonic network model best matched the atomistic MD simulation fluctuation projected along the distance between the coarse-grained sites (4), where it was enforced that the bond stiffness of every "identical bond" (i.e. between two beads of the same type and the same distance away in the filament structure) also be the same for symmetry reasons. The interface "stiffness" values used in this study are identical to our previous study (5).

The 3D position of the proteins ($\boldsymbol{G}^{(k)}$) and their local frame ($a^{(k)}$, $a^{(k)}$, $a^{(k)}$) are mapped to the global frame ($\mathbf{e_1}$, $\mathbf{e_2}$, $\mathbf{e_3}$) by a rotation matrix ($R^{(k)}$) (Figure S10A). The coordinates of an elastic bond end point ($\boldsymbol{M}^{(k)}$) on the surface of a protein k are defined by the vector ($\boldsymbol{X}^{(k)}$) that connects $\boldsymbol{G}^{(k)}$ to $\boldsymbol{M}^{(k}$. In the global frame this position is given by:

$$\boldsymbol{M} = \boldsymbol{G} + R(\boldsymbol{\psi}) \cdot \boldsymbol{X} \qquad (1)$$

The elastic bonds connecting two proteins are defined by harmonic potentials with an energy *E*. The magnitude of *E* depends on the bond stiffness (*S)*, the distance between the attachment points ($\left|\boldsymbol{M}^{(k_1,j)} - \boldsymbol{M}^{(k_2,j)}\right|$), and the resting length ($\lambda^{(k_1,k_2,j)}$) of the bond *j* between proteins k_1 and k_2 (Figure S10B) according to:

$$E_{elastic,j}^{(k_1,k_2)} = S/2\left(\left|\boldsymbol{M}^{(k_1,j)} - \boldsymbol{M}^{(k_2,j)}\right| - \lambda^{(k_1,k_2,j)}\right)^2 \qquad (2)$$

The total elastic energy of the interface between proteins k_1 and k_2 is given by the sum of the bond energies connecting the proteins (Figure S6B):

$$E_{elastic,int}^{(k_1,k_2)} = \sum_j E_{elastic,j}^{(k_1,k_2)} \qquad (3)$$

This energy represents the elastic energy strain energy of each interface. The energy of each interface at the initial configuration is 0.

Application of external load

Filaments (100 nm, with or without cofilin) were deformed in a series of small steps with imposed compressive, extensional, or torsional loads (Figure S6). Force balance equilibrium was maintained after each step using the Newton-Raphson method to iteratively minimize the force and torque by adjusting the position and rotation matrices for each protein within the filament until a predefined error tolerance was met. Inertial damping forces are neglected, as these are minor compared to elastic forces at this length scale.

Compression was imposed by bringing the filament ends closer until filament fragmentation. Filament ends were free to rotate. The boundary conditions for compression were chosen to approximate a filament segment within a longer, curved segment. Filaments were extended by moving the filament ends apart until fragmentation; filament ends were not allowed to rotate during extension. Twisting loads were applied by rotating filament ends about the filament axis and preventing axial movement, until filament fragmentation. The speeds of compression (60 nm/s), extension (10 nm/s), and twisting (720 degrees/s) were the same for all cofilin distributions.

Time steps in the simulation were variable and determined dynamically, but the rate of deformation was fixed (i.e. if the time step is reduced by half, the deformation is also reduced by half).

This was done to speed computation time in early stages of filament deformation. The default (and maximum) time step was set to be 2 ms. If more than 80 equilibration iterations were required before the equilibration tolerance was met for a given time step, the time step for the following deformation was decreased by 50% (to a minimum of 20 ns). If instead the equilibration was complete in few iterations (fewer than 5) the time step was increased 4-fold (up to a maximum of 2 ms). In practice, the time steps usually became shorter when bonds started breaking and the equilibrium filament shape changed in response.

The applied, external force and torque (imposed on N proteins) are coded via $3 \times N$ vectors. The internal forces and torques for each protein are the summation of the forces and torques applied by all attached bonds. Equilibrium is reached when all internal and external forces and torques are balanced for all proteins (i.e., $F_{int} + F_{ext} = 0$ and $T_{int} + T_{ext} = 0$).

SUPPORTING REFERENCES

1. McCullough BR*, et al.* (2011) Cofilin-linked changes in actin filament flexibility promote severing. *Biophys J* 101(1):151-159.
2. Fan J, Saunders MG, & Voth GA (2012) Coarse-graining provides insights on the essential nature of heterogeneity in actin filaments. *Biophys J* 103(6):1334-1342.
3. Phillips JC*, et al.* (2005) Scalable molecular dynamics with NAMD. *J. Comput. Chem.* 26:1781-1802.
4. Lyman E, Pfaendtner J, & Voth Ga (2008) Systematic multiscale parameterization of heterogeneous elastic network models of proteins. *Biophysical journal* 95:4183-4192.
5. Schramm AC*, et al.* (2017) Actin Filament Strain Promotes Severing and Cofilin Dissociation. *Biophys J* 112(12):2624-2633.

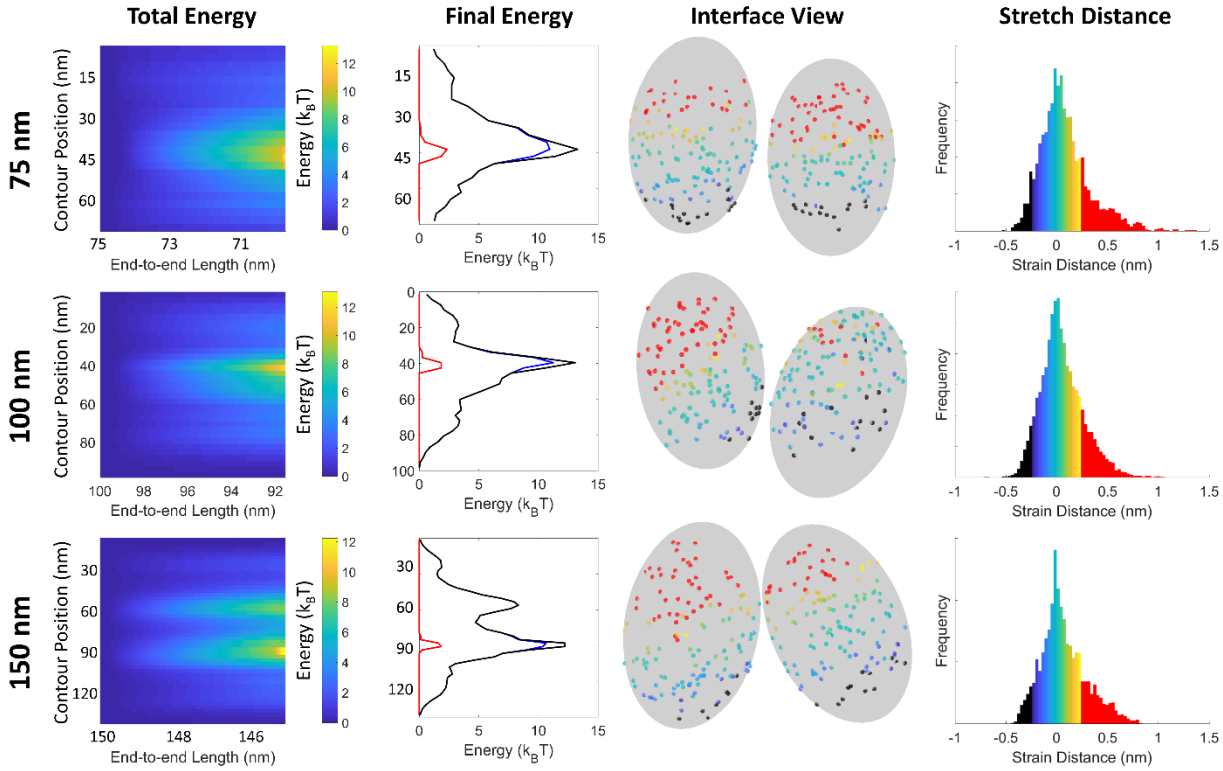

FIGURE S1 Effect of filament length (rows) on simulations of compressed actin filaments. The total energy column shows the energy across the filament vs the end-to-end displacement. The colors correspond to the adjacent colorbar. Final energy is the energy across the filament immediately prior to fragmentation. $E_{broken,fil}$ – red, $E_{elastic,fil}$ – blue, $E_{strain,fil}$ – black. The interface view shows the spatial strain on the interface immediately prior to fragmentation for an example simulation. The stretch distance column shows the cumulative histogram across 10 simulations. Positive values are stretched, negative values are compressed. The colors on the stretch distance histogram correspond to the bond colors for the interface view. Red bonds and bars on the histograms are broken bonds.

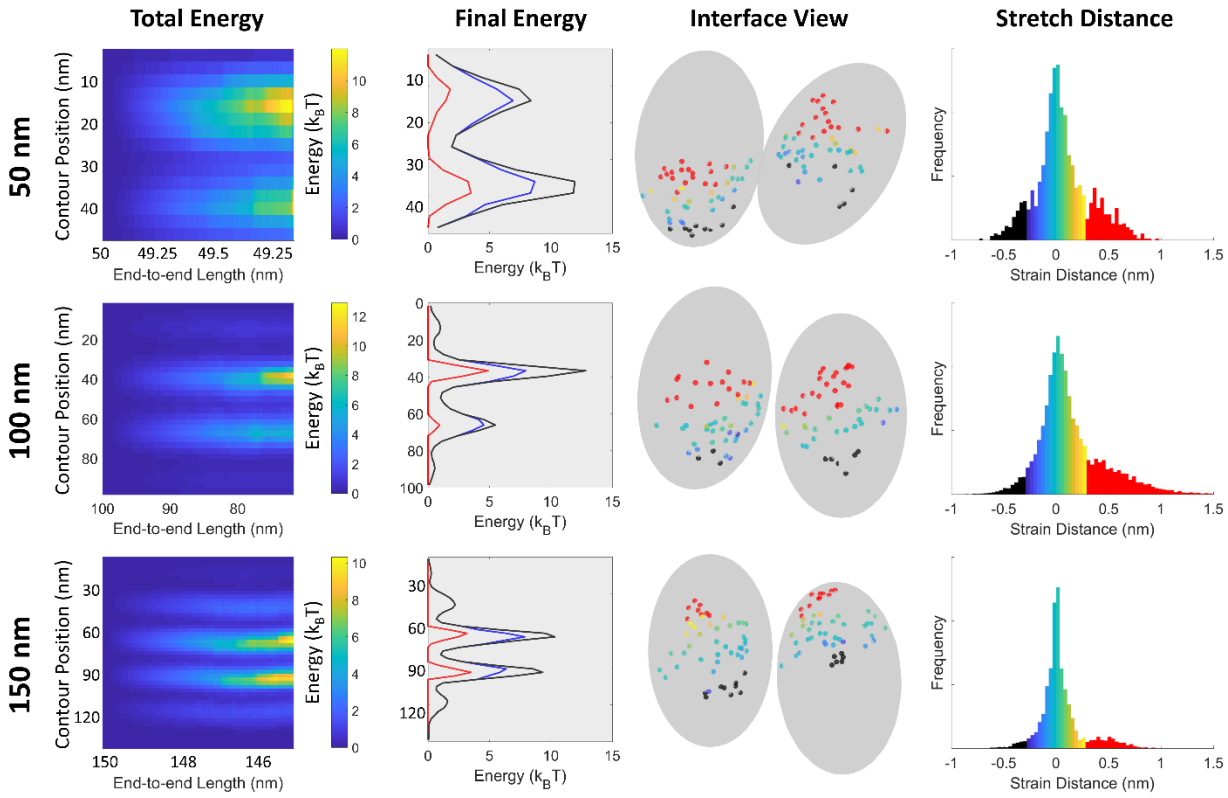

FIGURE S2 Effect of filament length (rows) on simulations of compressed cofilactin filaments. The total energy column shows the energy across the filament vs the end-to-end displacement. The colors correspond to the adjacent colorbar. Final energy is the energy across the filament immediately prior to fragmentation. $E_{broken,fil}$ – red, $E_{elastic,fil}$ – blue, $E_{strain,fil}$ – black. The interface view shows the spatial strain on the interface immediately prior to fragmentation for an example simulation. The stretch distance column shows the cumulative histogram across 10 simulations. Positive values are stretched, negative values are compressed. The colors on the stretch distance histogram correspond to the bond colors for the interface view. Red bonds and bars on the histograms are broken bonds.

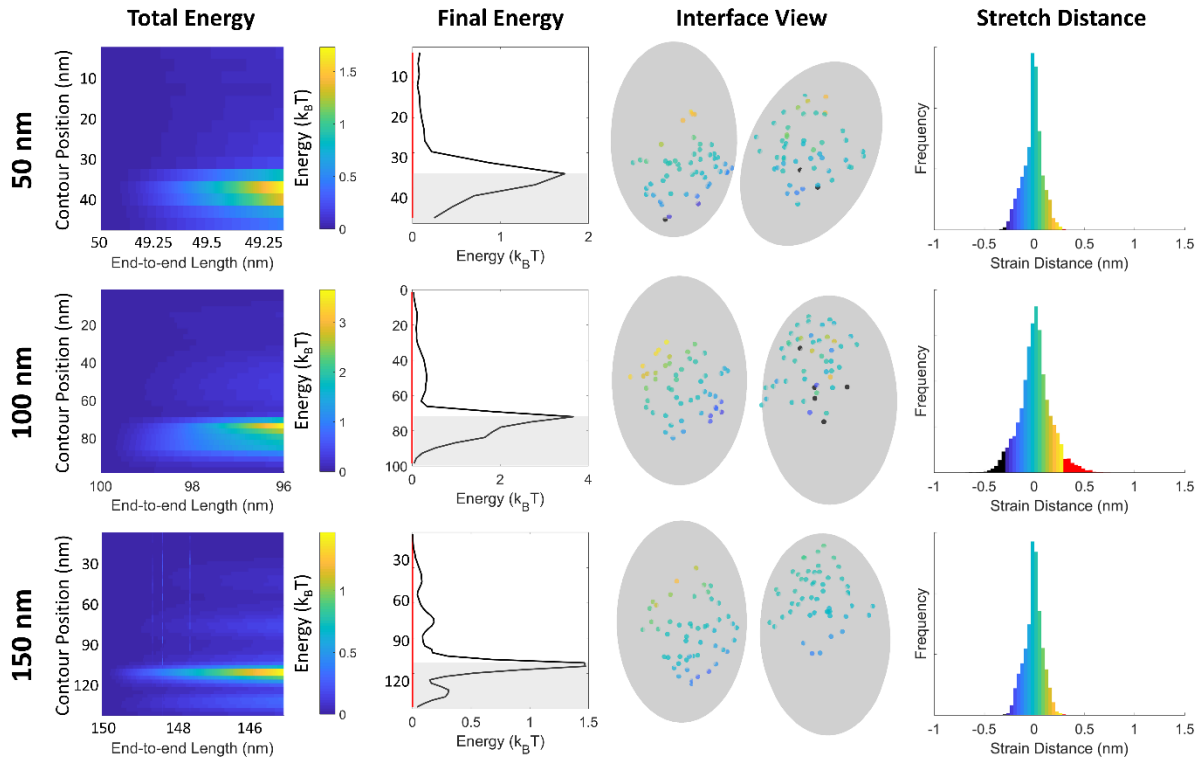

FIGURE S3 Effect of filament length (rows) on simulations of compressed filaments with a boundary. The total energy column shows the energy across the filament vs the end-to-end displacement. The colors correspond to the adjacent colorbar. Final energy is the energy across the filament immediately prior to fragmentation, and the shading shows where cofilin is located. $E_{broken,fil}$ – red, $E_{elastic,fil}$ – blue, $E_{strain,fil}$ – black. The interface view shows the spatial strain on the interface immediately prior to fragmentation for an example simulation. The stretch distance column shows the cumulative histogram across 10 simulations. Positive values are stretched, negative values are compressed. The colors on the stretch distance histogram correspond to the bond colors for the interface view. Red bonds and bars on the histograms are broken bonds.

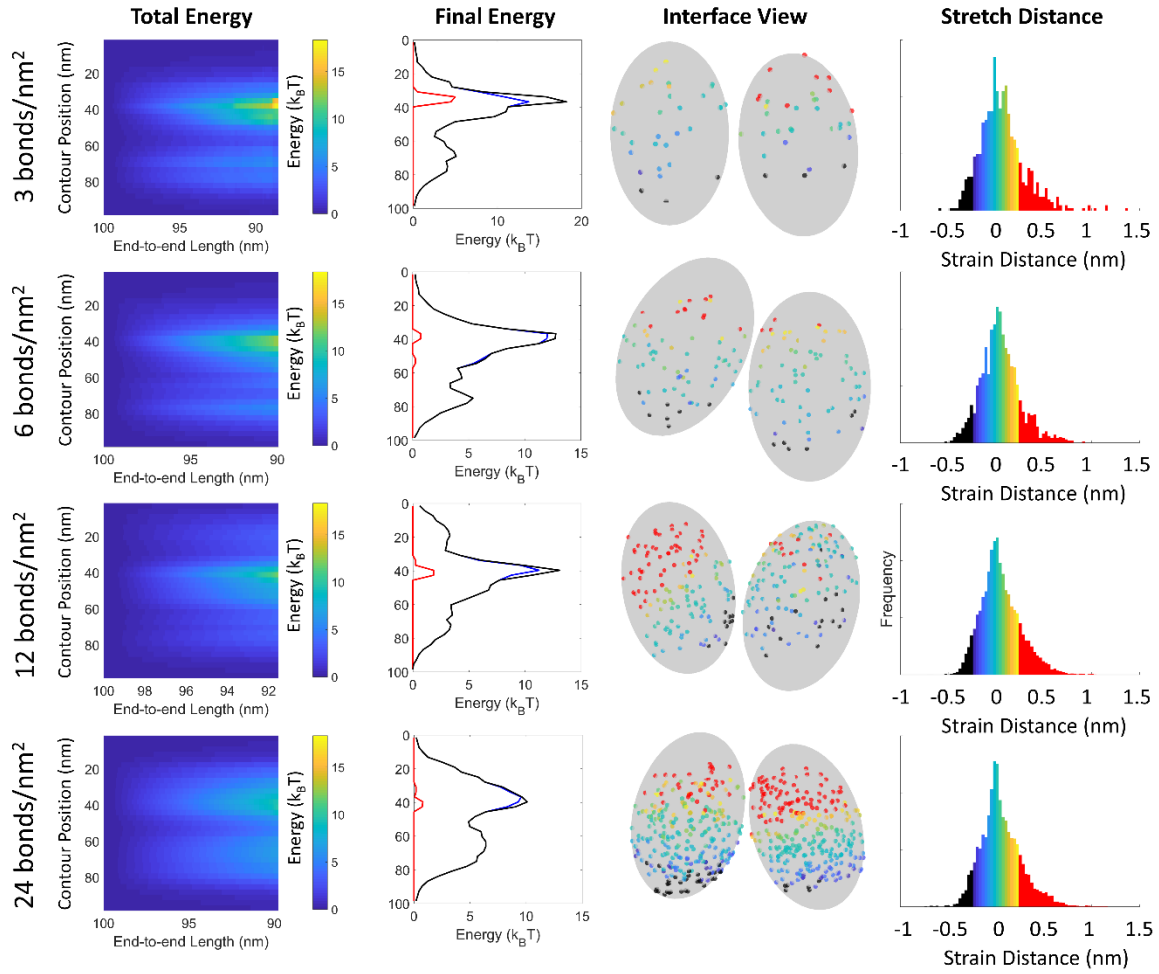

FIGURE S4 Effect of bond density (rows) on simulations of compressed actin filaments. The "Total Energy" column shows the energy across the filament vs the end-to-end displacement. The colors correspond to the adjacent colorbar. Final energy is the energy across the filament immediately prior to fragmentation. $E_{broken,fil}$ – red, $E_{elastic,fil}$ – blue, $E_{strain,fil}$ – black. The interface view shows the spatial strain on the interface immediately prior to fragmentation for an example simulation. The stretch distance column shows the cumulative histogram across 10 simulations. Positive values are stretched, negative values are compressed. The colors on the stretch distance histogram correspond to the bond colors for the interface view. Red bonds and bars on the histograms are broken bonds. 12 bonds/nm^2 was the bond density used for simulations in the main text.

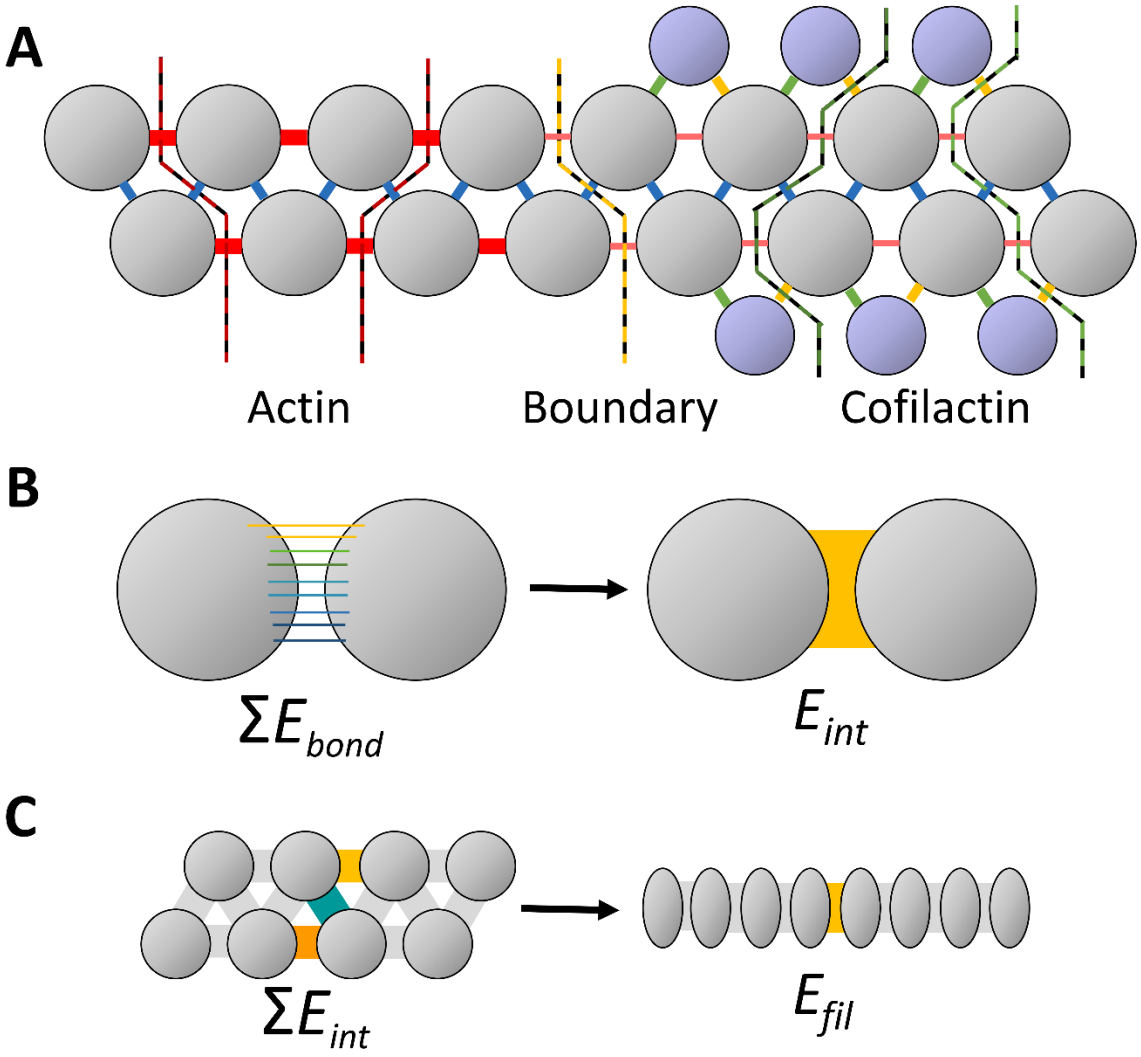

FIGURE S5 A) Filament interface diagram. Actin (grey) and cofilin (purple) molecules are shown near an actin-cofilactin interface. Filaments connections include longitudinal (red), lateral (blue), and cofilin-actin interfaces towards the pointed (green) and barbed (yellow) end. The light red, thinner longitudinal bonds shows where the weaker longitudinal interface of cofilactin is applied. Lines show a subset of the filament cross-sections over which the filament energy is calculated for fragmentation rate calculations. For both bare actin and cofilactin there exists a cross-section for each lateral (blue) interface. Within cofilactin, the cross-section goes through one lateral (blue), two longitudinal (red) and two cofilin-actin interfaces. We choose to always go through the cofilin-actin interactions on the barbed side, as these interactions are weaker (Table S1). B) Illustration of Equation 3. C) Illustration of Equation 2.

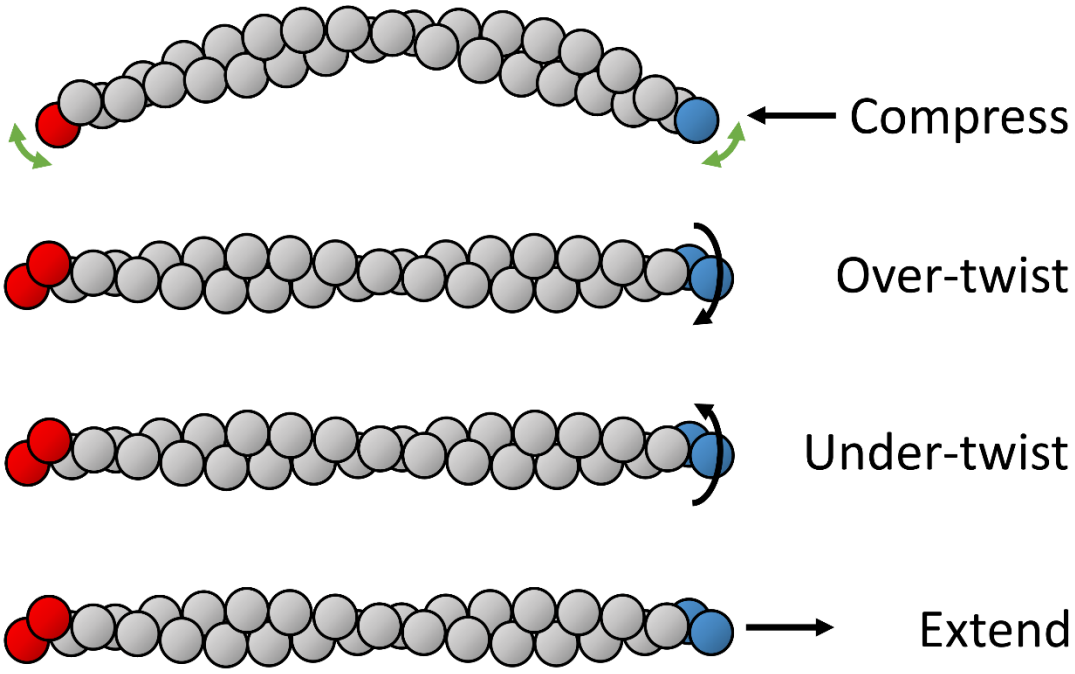

FIGURE S6 Applied deformations to filaments. For each given deformation, red monomers are fixed in space. The force applied for each type of deformation is shown by the black arrows and applied to the blue monomers. Green arrows indicate a freedom of rotation for the colored subunits. The grey subunits shown have no external constraints.

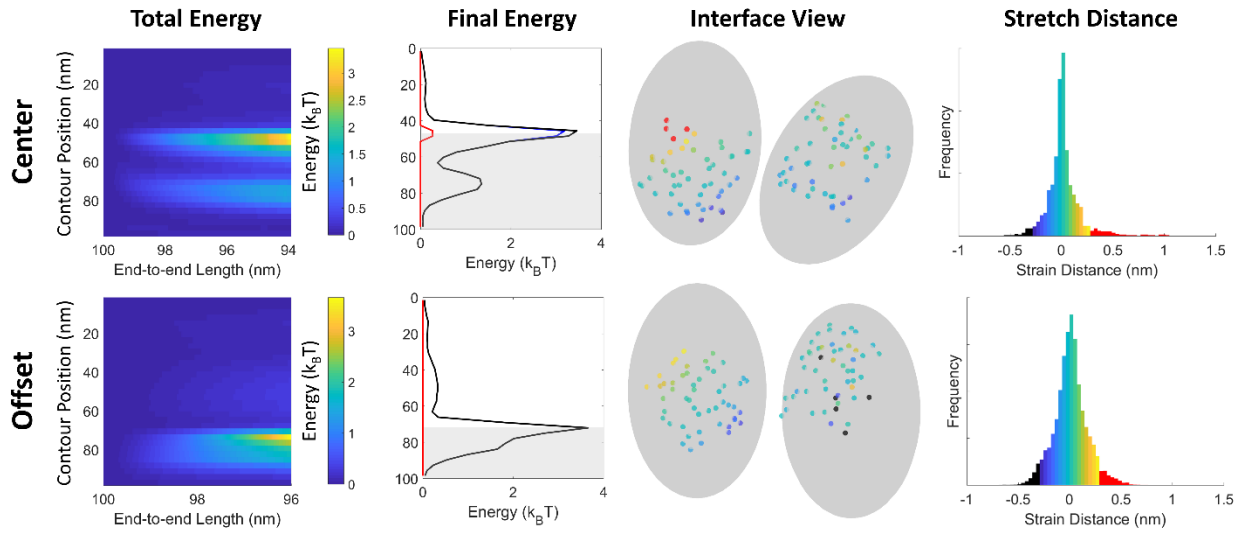

FIGURE S7 Effect of the boundary placement of compressed filaments. The total energy column shows the energy across the filament vs the end-to-end displacement. The colors correspond to the adjacent color bar. Final energy is the energy across the filament immediately prior to fragmentation, and the shading shows where cofilin is located. $E_{broken,fil}$ – red, $E_{elastic,fil}$ – blue, $E_{strain,fil}$ – black. The interface view shows the spatial strain on the interface immediately prior to fragmentation for an example simulation. The stretch distance column shows the cumulative histogram across 10 simulations. Positive values are stretched, negative values are compressed. The colors on the stretch distance histogram correspond to the bond colors for the interface view. Red bonds and bars on the histograms are broken bonds.

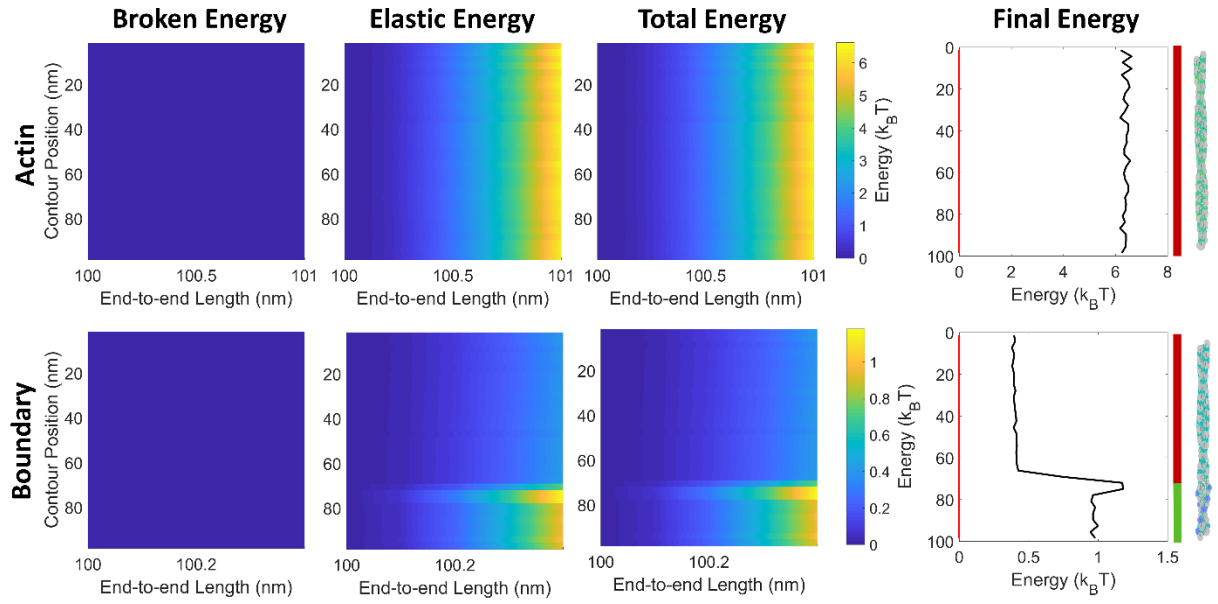

FIGURE S8 Simulations of a 100 nm extended bare actin filament (top rows) and a filament with a boundary (bottom rows). Final energy corresponds to the energy just prior to rupture. $E_{broken,fil}$ – red, $E_{elastic,fil}$ – blue, $E_{strain,fil}$ – black. Lines to the right of the final energy show the location of actin (red) and cofilactin (green) for each distribution. The final filament configuration is shown on the right edge of the figure.

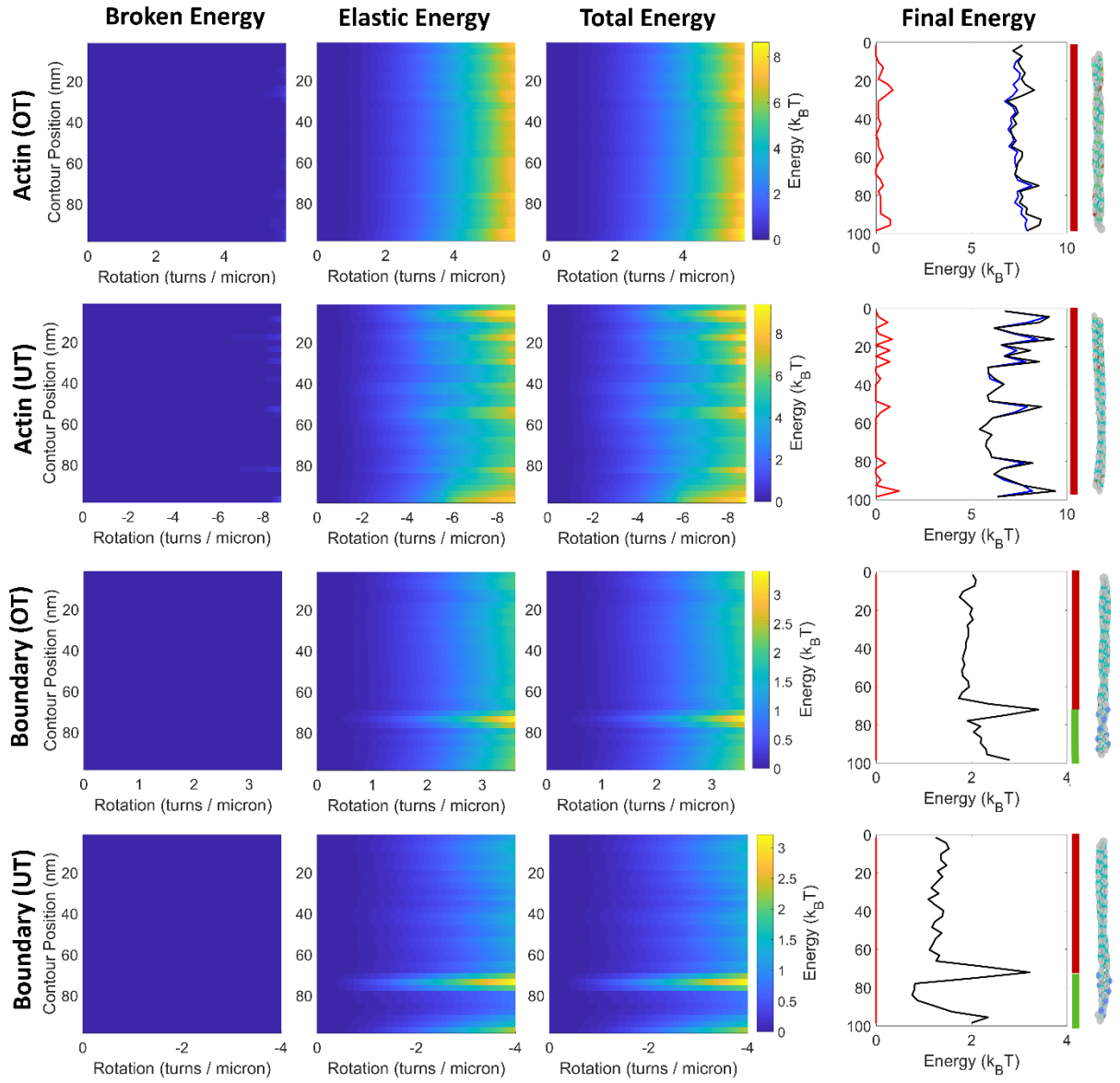

FIGURE S9 Simulations of a 100 nm twisted bare actin filament (top two rows) and a filament with a boundary (bottom two rows). Filaments are either over- (rows 1 and 3, OT) or under-twisted (rows 2 and 4, UT). Final energy corresponds to the energy just prior to rupture. $E_{broken,fil}$ – red, $E_{elastic,fil}$ – blue, $E_{strain,fil}$ – black. Lines to the right of the final energy show the location of actin (red) and cofilactin (green) for each distribution. The final filament configuration is shown on the right edge of the figure.

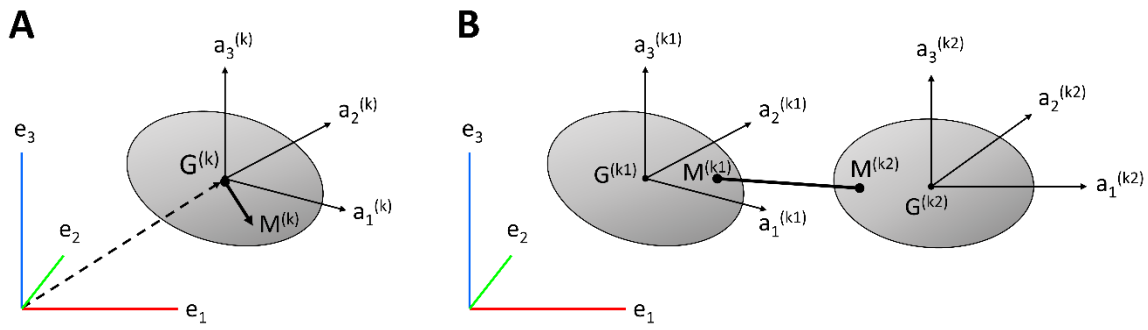

FIGURE S10 A) Depiction of the center of mass vector (dashed line, $\mathbf{G}^{(k)}$), local reference frame vectors ($\mathbf{a}^{(k)}$), and the vector from the mass center to an attachment point on protein *k* ($\mathbf{M}^{(k)}$). B) Diagram showing an example of a bond connecting two proteins *k1* and *k2*.

SUPPLEMENTAL MOVIES

Movies of filament fragmentation. Bond colors change according to their strain (see Figure S1 histograms for corresponding distances) and become red upon bond rupture. Movie framerate is set to make movies 3 seconds long. Step sizes are variable, so temporal information is not preserved.

MOVIE S1 Bare actin filament compression

MOVIE S2 Cofilactin filament compression

MOVIE S3 Actin-cofilactin boundary filament compression

MOVIE S4 Bare actin filament extension

MOVIE S5 Actin-cofilactin boundary filament extension

MOVIE S6 Bare actin filament over-twisting

MOVIE S7 Bare actin filament under-twisting

MOVIE S8 Actin-cofilactin boundary filament over-twisting

MOVIE S9 Actin-cofilactin boundary filament under-twisting

TABLE S1 Model filament parameters

Actin filament	Value
Filament period	71.2 nm[a]
Number of actin subunits in one period	26[a]
Rotation per subunit	166.1° [a]
Rise per actin subunit (same strand)	5.52 nm[a]
Actin filament interaction radius	1.8 nm[a]
Actin subunit dimensions	5.1 x 5.1 x 3.3 nm[a]
Actin-actin longitudinal interface stiffness	582 k_BT/nm^2 [a,c]
Actin-actin lateral interface stiffness	392 k_BT/nm^2 [a,c]
Actin-actin longitudinal interface area	11.2 nm^2 [a,d]
Actin-actin lateral interface area	3.9 nm^2 [a,d]
Bond density	12 bonds/nm^2
Cofilactin filament	
Filament period	55.2 nm[b]
Number of actin subunits in one period	20.1[b]
Rotation per subunit	162.1° [b]
Rise per actin subunit (same strand)	5.49 nm[b]
Actin filament interaction radius	1.7 nm[b]
Cofilin radius (distance from filament centerline)	3.7 nm[b]
Actin subunit dimensions	5.1 x 5.1 x 3.3 nm[a]
Cofilin subunit dimensions	3.1 x 3.3 x 1.8 nm[b]
Actin-actin longitudinal interface stiffness	169 k_BT/nm^2 [b,c]
Actin-actin lateral interface stiffness	429 k_BT/nm^2 [b,c]
Actin-actin longitudinal interface area	4.3 nm^2 [b,d]
Actin-actin lateral interface area	3.7 nm^2 [b,d]
Actin-cofilin interface stiffness, towards pointed end	157 k_BT/nm^2 [b,c]
Actin-cofilin interface stiffness, towards barbed end	204 k_BT/nm^2 [b,c]
Actin-cofilin interface area, towards pointed end	10.3 nm^2 [b,d]
Actin-cofilin interface area, towards barbed end	7.4 nm^2 [b,d]
Bond density	12 bonds/nm^2
Severing parameters	
Filament severing rate (actin and cofilactin)	500e-9 s^{-1} $monomer^{-1}$
Bond rupture distance (actin)	0.24 nm
Bond rupture distance (cofilactin)	0.29 nm

[a] Measured from PDB file 3J8I.

[b] Measured from PDB file 3J0S.

[c] Reference 10

[d] NIH Supercomputing resource, http://helixweb.nih.gov/structbio/basic.html

TABLE S2 Pre-fragmentation interface energies

Deformation	Filament Type	Interface Type	$E_{elastic,int}/\Delta G^{\ddagger}_{int,native}$ (pre-fragmentation)	$E_{broken,int}/\Delta G^{\ddagger}_{int,native}$ (pre-fragmentation)
Compression (N = 50)	Actin	Longitudinal	0.33 ± 0.03	0.21 ± 0.05
		Lateral	0.08 ± 0.05	0 ± 0
	Cofilactin	Longitudinal	0.37 ± 0.09	0.42 ± 0.08
		Lateral	0.19 ± 0.07	0.04 ± 0.06
		Cofilin-Actin	0.17 ± 0.05	0.16 ± 0.08
	Boundary	Longitudinal	0.30 ± 0.05	0.063 ± 0.062
		Lateral	0.040 ± 0.015	0 ± 0
Extension (N = 20)	Actin	Longitudinal	0.40 ± 0.05	0 ± 0
		Lateral	0.01 ± 0.005	0 ± 0
	Boundary	Longitudinal	0.26 ± 0.06	0 ± 0
		Lateral	0.008 ± 0.003	0 ± 0
Over-twist (N = 20)	Actin	Longitudinal	0.17 ± 0.02	0.18 ± 0.11
		Lateral	0.22 ± 0.09	0.001 ± 0.005
	Boundary	Longitudinal	0.20 ± 0.06	0.01 ± 0.02
		Lateral	0.06 ± 0.02	0 ± 0
Under-twist (N = 20)	Actin	Longitudinal	0.24 ± 0.2	0.09 ± 0.03
		Lateral	0.35 ± 0.07	0.28 ± 0.07
	Boundary	Longitudinal	0.17 ± 0.03	0.02 ± 0.03
		Lateral	0.09 ± 0.04	0 ± 0

TABLE S3 Pre-fragmentation filament energies and rupture forces

Deformation	Filament Type	$E_{elastic,fil}/\Delta G^{\ddagger}_{native}$ (pre-fragmentation)	$E_{broken,fil}/\Delta G^{\ddagger}_{native}$ (pre-fragmentation)	Rupture Force (pN)
Compression (N = 50)	Actin	0.26 ± 0.03	0.15 ± 0.03	35.6 ± 0.9
	Cofilactin	0.24 ± 0.03	0.19 ± 0.06	7.2 ± 0.2
	Boundary	0.16 ± 0.02	0.028 ± 0.027	13.6 ± 0.7
Extension (N = 20)	Actin	0.30 ± 0.03	0 ± 0	760 ± 20
	Boundary	0.029 ± 0.007	0 ± 0	290 ± 30
				Rupture Torque (pN nm)
Over-twist (N = 20)	Actin	0.19 ± 0.02	0.13 ± 0.08	460 ± 30
	Boundary	0.12 ± 0.03	0.004 ± 0.008	250 ± 40
Under-twist (N = 20)	Actin	0.27 ± 0.01	0.14 ± 0.03	350 ± 30
	Boundary	0.13 ± 0.03	0.01 ± 0.01	200 ± 50

TABLE S4 Length effects on compressive simulations

Filament type (length (nm))	Fragmentation Angle (degrees)	$E_{elastic,int}/\Delta G^{\ddagger}_{int,native}$ (pre-fragmentation)	$E_{broken,int}/\Delta G^{\ddagger}_{int,native}$ (pre-fragmentation)	Rupture Force (pN)
Actin (75)	48 ± 3	0.27 ± 0.02	0.18 ± 0.03	53.1 ± 1.4
Actin (100)	63 ± 4	0.26 ± 0.03	0.15 ± 0.03	35.6 ± 0.9
Actin (150)	88 ± 7	0.25 ± 0.01	0.18 ± 0.07	15.4 ± 0.1
Cofilactin (50)	78 ± 9	0.23 ± 0.03	0.11 ± 0.04	21.8 ± 0.7
Cofilactin (100)	123 ± 12	0.24 ± 0.03	0.19 ± 0.06	7.2 ± 0.2
Cofilactin (150)	161 ± 9	0.19 ± 0.03	0.12 ± 0.04	3.7 ± 0.1
Boundary (50)	20 ± 3	0.09 ± 0.02	0.0 ± 0.0	26.4 ± 2.6
Boundary (100)	49 ± 3	0.16 ± 0.02	0.028 ± 0.027	13.6 ± 0.7
Boundary (150)	38 ± 5	0.07 ± 0.02	0.0 ± 0.0	7.2 ± 0.2

TABLE S5 Density effects on compressed actin filaments

Density	Fragmentation Angle (degrees)	$E_{elastic,int}/\Delta G^{\ddagger}_{int,native}$ (pre-fragmentation)	$E_{broken,int}/\Delta G^{\ddagger}_{int,native}$ (pre-fragmentation)	Rupture Force (pN)
3 links / nm^2	59.6 ± 7	0.31 ± 0.5	0.13 ± 0.6	27.7 ± 1.5
6 links / nm^2	62.9 ± 6	0.30 ± 0.3	0.14 ± 0.5	30.3 ± 0.7
12 links / nm^2	63 ± 4	0.26 ± 0.03	0.15 ± 0.03	35.6 ± 0.9
24 links / nm^2	66 ± 4	0.28 ± 0.03	0.16 ± 0.02	32.2 ± 0.3